RSC Advances

ROYAL SOCIETY OF CHEMISTRY

www.rsc.org/advances

Journal Name

RSCPublishing

ARTICLE

Selective growth of carbon nanotubes on boron-doped diamond for electrochemical biosensor application

Cite this: DOI: 10.1039/x0xx00000x

Seung-Koo Lee,[a,d] Min-Jung Song,[b,d] Jong-Hoon Kim,[a,c] Young-Kyun Lim,[a] Yoon-Soo Chun[a] and Dae-Soon Lim[a]*

Received 00th January 2012,
Accepted 00th January 2012

DOI: 10.1039/x0xx00000x

www.rsc.org/

A method for selective and direct growth of multi-wall carbon nanotubes (MWCNTs) on the boron-doped diamond (BDD) was developed using electrostatic self-assembly of catalytic nanoparticles via conventional photolithography method. As catalysts, stainless steel 316L (SUS316L) nanoparticles consisted of catalytic ions such as Fe and Ni were introduced. As-grown MWCNTs had a porous random-network structure that was suitable for an electrochemical biosensor application. The electrochemical properties of the electrodes were characterized using cyclic voltammetry and electrochemical impedance spectroscopy. The effective surface area of the as-developed BDD/MWCNT electrode was larger than that of the BDD electrode and its electron transfer resistance was about 40 Ω, which is around 16 times higher than that of BDD electrode. To evaluate the biosensing performance, glucose was chosen as a target analyte. The BDD/MWCNT electrode exhibited a higher sensitivity of 7.2 μA/mM·cm^2 (R=0.9943) with a wider linear range than did the BDD electrode, because of the synergistic effect between the MWCNTs and BDD.

Introduction

Carbon nanotube (CNT)[1-3] has been used for extensive applications in various fields because of their unique structure, excellent conductivity, high chemical stability, large surface area, and high catalytic activity. In electrochemical application, particularly, CNT-based electrodes exhibit enhanced electrochemical sensor performance, yielding high sensitivity, a wide linear range, and fast response times.[4-6]

Recently, boron-doped diamond (BDD) film[7-11] has been used as an active electrode for various electrochemical sensors because of its low capacitive current, large potential window, and low adsorption of organic contaminants. These unique properties lead to an enhanced signal-to-noise ratio (S/N) and a low detection limit. In spite of these outstanding properties, however, BDD shows low sensitivity for biosensor applications. To overcome the performance limitation, several researchers performed the modification of the BDD film with various methods, such as nanomaterial decoration, metal ion implantation, plasma treatment, etc.[12-15]

The CNT/diamond hybrid structure can overcome the limitation of the nanostructure formation of the BDD and exhibit the synergistic properties. Several researchers fabricated the CNTs on diamond structures by various methods.[16-20] Varshney et al. showed CNTs on diamond structure exhibits enhanced emission properties and long-term stability as compared CNTs alone.[16] Recently, Herbert et al. presented the composite nanomaterial of CNTs on BDD fabricated using partially embedded catalyst in nanocrystalline diamond film and estimated electrochemical properties.[20] However, the evaluation of the biosensing performance with CNTs on BDD structure has not yet been explored.

To achieve CNT-based sensor devices, patterning of the CNTs with a three-dimensional (3D) porous network structure is required to provide facile access to the analytes for electrochemical measurement.[21] Many researchers have studied patterning of CNTs using a variety of methods, such as template-based synthesis[22], transferring techniques[23], direct etching [24], microcontact printing[25], direct growth on a patterned catalyst[26,27], and so on. Among the diverse CNT patterning methods, direct growth with a patterned catalyst is the most promising technique for fabricating a 3D porous network structure. However, the conventional selective growth techniques reported in the literature require complicated additional processes to make a catalyst layer on the substrate, such as deposition and heat treatment. Thus, development of a simple and cost-effective CNT patterning method is required.

In this study, we describe the method for site-selective and direct growth of the multi-wall CNTs (MWCNTs) on the BDD using electrostatic self-assembly (ESA) of catalytic nanoparticles. In addition, the electrochemical biosensing performances were evaluated with as-developed MWCNTs on BDD electrode pattern. Glucose was chosen as a target analyte. Combining porous random-networked MWCNTs and BDD (BDD/MWCNT) is expected to

enhance the electrochemical properties as well as sensing performances.

Experimental

Reagents and chemicals

Stainless steel 316L (SUS316L) nanoparticles with an average individual particle size of 100 nm were purchased from Heyuan Zhonglian Nanotechnology Co., Ltd. (Guangdong, China). Acetone, ethanol, potassium ferricyanide ($K_4Fe(CN)_6$), potassium hexacyanoferrate (III) ($K_3Fe(CN)_6$), potassium chloride, and sulfuric acid were obtained from Samchun Chemicals (Gyeonggi-do, Korea). AZ1512 photoresist (PR) solution, its developer AZ500 MIF, poly sodium 4-styrene sulfonate (PSS, Mw: 70,000), and polyethyleneimine (PEI, Mw: 2,000) were purchased from Sigma-Aldrich Chemical Co. (St. Louis, USA). A glutaraldehyde (GA) solution (25% in water) was purchased from Kanto Chemical (Tokyo, Japan). 3-Aminopropyltriethoxysilane (APTES) was obtained from Aldrich Chemical (St. Louis, USA). D-Glucose and glucose oxidase (GO_x; E.C. 1.1.3.4, 200 U/g) from *Aspergillus niger* were purchased from Sigma Chemicals (St. Louis, USA). All stock solutions were dissolved in a 0.05 M phosphate buffer (PB) solution at pH 7.0. Diluted glucose solutions were prepared from a stock solution just before use.

Characterization

The morphology and structure of the as-grown MWCNTs were determined using field-emission scanning electron microscopy (FE-SEM, Hitachi S-4800), field-emission transmission electron microscopy (FE-TEM, Tecnai 20), and Raman spectroscopy with a 514.5 nm Ar-ion laser (Horiba Jobin Yvon; T64000). All electrochemical measurements were performed using a VersaSTAT 3 instrument (Princeton Applied Research, USA) connected to a three-electrode cell. The three-electrode system consisted of a platinum (Pt) wire as a counter electrode, an Ag/AgCl reference electrode, and the modified BDD electrodes (a bare BDD and BDD/MWCNT) as the working electrodes.

Fabrication of the BDD/MWCNT electrode pattern

Figure 1 shows schematic procedure for BDD/MWCNT electrode pattern (target pattern). Before the MWCNT growth, a BDD electrode pattern was fabricated using an ESAND method and conventional photolithography process. For precise BDD pattern, agglomerated nanodiamond particles were dispersed using attrition milling process with zirconia beads of 2 kg (mixture of 0.1 mm and 0.3 mm in diameter) at the velocity of 1000 rpm for 6 hrs. During the milling process, highly dispersed and anionic PSS-coated nanoparticles (PSS-NDs) were obtained. Details for BDD patterning procedure were shown in the previous study.[28] BDD was synthesized using a hot-filament chemical vapor deposition (HFCVD) system with a gas mixture of 1 % CH_4 in H_2 and diluted B_2H_6 in H_2 (B/C ratio = 5000 ppm). Before site-selective and direct growth of MWCNTs on the sensing part of the BDD electrode pattern, Si_3N_4 was deposited on the edge of the BDD electrode pattern using plasma-enhanced CVD to isolate the sensing part against other environments. After this, SUS316L nanoparticles were coated on the sensing part of the BDD electrode using ESA and photolithography method. Anionic PSS polymers were coated on the cationic BDD electrode surface for spontaneous electrostatic interaction between the cationic SUS316L nanoparticles and the BDD surface. Therefore, the PSS-coated BDD electrode was dipped in the cationic SUS316L nanoparticle suspension for 1 hr. After simple lift-off process, the BDD electrode pattern on which the cationic SUS316L nanoparticles were attached at sensing part was fabricated. MWCNTs were directly grown on the surfaces of the SUS316L nanoparticles using thermal CVD. The Synthesis conditions of the MWCNTs were the same as explained above.

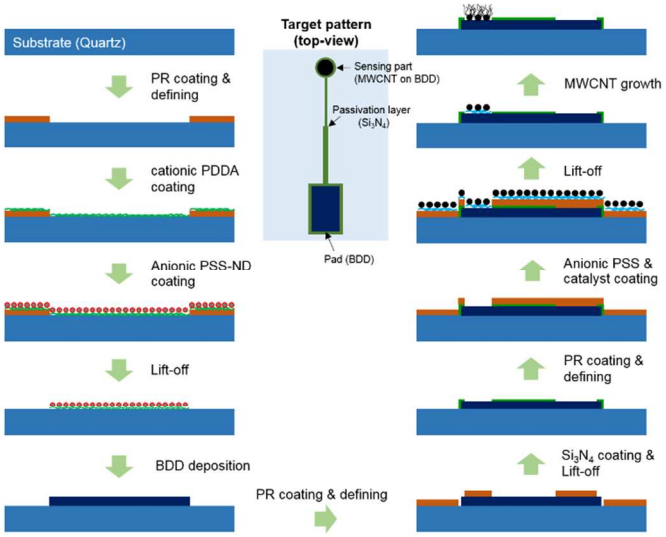

Figure 1. Fabrication procedure of the BDD/MWCNT electrode pattern.

Immobilization of GO_x on the working electrodes

To test the electrodes as electrochemical sensors, glucose was chosen as a target analyte. GO_x was immobilized on the modified electrodes by covalent binding for the detection of glucose.[29] This procedure is briefly explained in Fig.2. O_2 plasma treatment was carried out to produce an oxygen-terminated surface on the MWCNT. GA was used as a linker to connect the APTES with the enzyme, which forms an amide linkage between the aldehyde group of the GA and the amino group of the APTES. GO_x was immobilized on the modified MWCNT by an amide bond between another aldehyde group of the GA and the N-terminus of GO_x. As the same method introduced above, immobilization of GO_x on the BDD surface was conducted to compare the sensing performances.

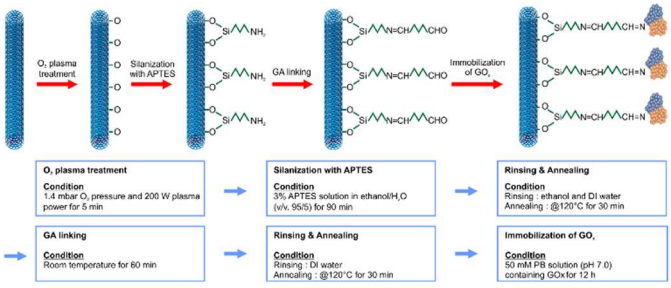

Figure 2. Schematic illustration of the immobilization of GO_x on the MWCNT surface.

Results and discussion

Figure 3(a) shows as-deposited BDD thin film. The thickness of the BDD film was about 200 nm. In the Raman spectra (Fig.3(b)), sp^3 diamond peak at 1325 cm^{-1} shifted from 1332 cm^{-1} by boron impurities and nanocrystalline diamond (NCD) peaks at 1140 cm^{-1} and 1480 cm^{-1} confirmed that as-grown film was consisted of diamond phase.

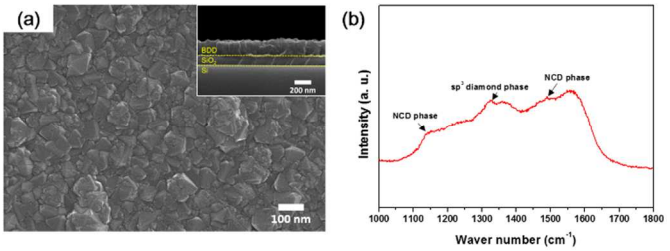

Figure 3. (a) SEM image of the as-deposited BDD thin film (inset: cross-sectional view of the BDD thin film), (b) Raman spectra of the BDD thin film.

MWCNTs grown selectively on the BDD electrode pattern were prepared to estimate the biosensing performance (Fig. 4). The BDD pattern was fabricated on a quartz substrate using ESAND and HFCVD. Then, a silicon nitride (Si_3N_4) passivation layer was deposited by photolithography at the edge of the BDD pattern. The as-prepared sensor consisted of the 1-mm-diameter detection part (circle pattern) with the MWCNTs (Fig.4(b)) and the bonding pad part (Fig.4(c)). Figure 4(d) and (e) show SEM images of the synthesized MWCNTs on the detection part. The MWCNTs had a 3D porous network structure and the thickness of MWCNT layer was about 8 μm. As-grown MWCNTs were adhered well to the BDD surface.

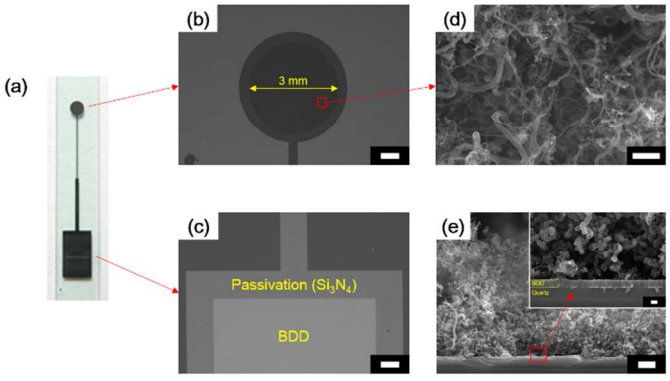

Figure 4. Optical and SEM images of MWCNTs on a BDD electrode; (a) BDD/MWCNT electrode, (b) selectively grown MWCNTs on the active site of the BDD pattern, (c) bonding pad of the MWCNT on BDD electrode, (d) high-resolution SEM image of the 3D-networked MWCNTs, and (e) cross-sectional view of the BDD/MWCNT electrode. Scale bars, 200 μm in (b) and (c), 500 nm in (d), and 2 μm in (e), and 100 nm in inset (e).

The growth phenomenon of the MWCNTs on the catalytic SUS316L nanoparticle were analyzed by SEM (Fig.5). A bare SUS316L nanoparticle is spherical shape with smooth surface and its average size is about 150 nm (Fig.5(a)). During the thermal CVD process for MWCNT growth, nano-sized hills were generated on the surface of the SUS316L nanoparticle at 750 °C (Fig.5(b)). As shown in Fig.5(c), one SUS316L nanoparticle had several MWCNTs with different diameters of 20 ~ 100 nm. Through the generated hills, several MWCNTs from one SUS316L nanoparticle were grown (some-to-one pathway) by diffusion of carbon atoms through C_2H_2 decomposition, obtaining the 3D porous network MWCNTs with various diameters. It was considered that the diameter of the as-grown MWCNT is related to the size of the generated hills.[30]

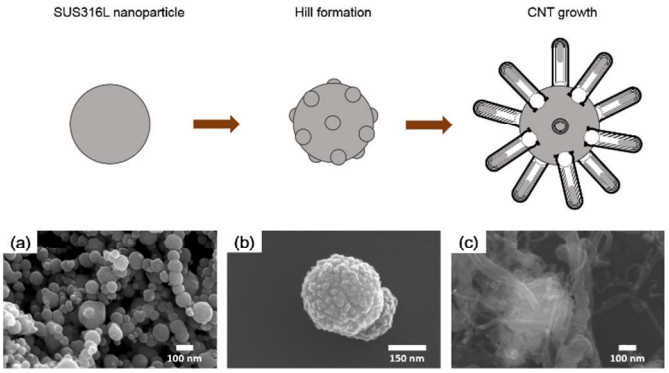

Figure 5. Schematic illustration of MWCNTs on SUS316L nanoparticle according to each steps and corresponded SEM images of (a) bare SUS316L nanoparticles, (b) heat-treated SUS316L nanoparticles at 750 °C and (c) MWCNT-grown SUS316L nanoparticle.

Raman analysis was performed for estimation of the crystalline quality of the MWCNT as shown in Fig.6. As-grown MWCNTs have two main peaks around 1571 cm^{-1} (G-band) and 1340 cm^{-1} (D-band). The G-band as tangential mode indicates the ordered carbon and the D-band characterizes the structural forms of disordered sp^2 carbon. The small ratio of D-band/G-band as a good indicator of the quality means low defect level in the atomic carbon structure for the sample.[31] This ratio of 0.82 for the as-grown MWCNT indicates a high quality of the structural defects.

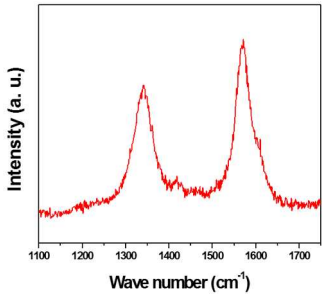

Figure 6. Raman spectra of the as-grown MWCNTs.

For the characterization of the electrochemical properties, the modified electrodes were examined by cyclic voltammetry (CV) and electrochemical impedance spectroscopy (EIS) in a 0.1 M KCl solution containing 5 mM $Fe(CN)_6^{3-/4-}$. Figure 7(a) shows the CVs of bare BDD and a BDD/MWCNT electrode. For the bare electrode, the anodic peak potential (E_{pa}) was 0.398 V (i_{pa} = 0.435 mA/cm^2) and the cathodic peak potential (E_{pc}) was 0.113 V (i_{pc} = -0.587 mA/cm^2), yielding a peak-to-peak separation (ΔE_p) of 0.285 V. The BDD/MWCNT electrode showed an increase in the oxidation peak current density (i_{pa} = 0.660 mA/cm^2 and E_{pa} = 0.337 V) and a decrease in the cathodic peak current density (i_{pc} = -0.570 mA/cm^2 and E_{pc} = 0.17 V), with a peak potential separation (ΔE_p) of approximately 0.167 V. The improved peak current density includes an increase of the effective surface area and the small ΔE_p leads to direct electron transfer between the electrode and redox species. This result confirms that the BDD/MWCNT electrode exhibited an enhanced signal and accelerated electron transfer due to synergistic effects of the MWCNTs and BDD.

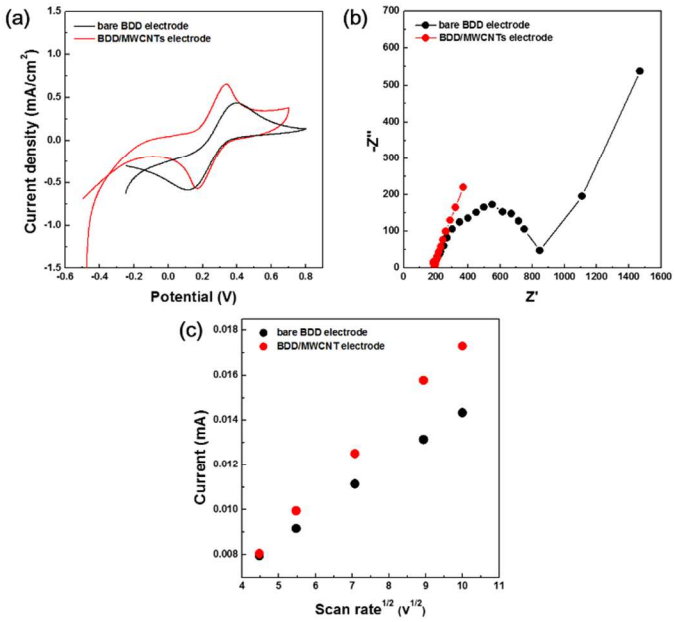

Figure 7. (a) Cyclic voltammograms of a bare BDD and the BDD/MWCNT electrodes in a solution of 10 mM $Fe(CN)_6^{3-/4-}$ containing 3 M KCl at 50 mV/s. (b) Nyquist plot of the EIS for the electrodes in a solution of 5 mM $Fe(CN)_6^{3-/4-}$ containing 0.1 M KCl at 0.24 V. (c) I_p vs. $v^{1/2}$ plots for the determination of the effective surface area of the electrodes.

An EIS study of the electrodes was also carried out over a frequency range of 10^{-2} to 10^5 Hz, with an applied sine wave potential with an amplitude of 5 mV and a formal potential of the system of 0.24 V as shown in Fig.7(b). A typical Nyquist plot of the impedance spectra consists of the real (x-axis) and imaginary (y-axis) parts of the cell impedance and is divided into a semicircle portion and a linear portion. Generally, the semicircle portion in the high-frequency range and the linear portion in a lower frequency range represent the electron-transfer-limited process and the diffusion-limited process, respectively. The diameter of the semi-circle indicates the electron-transfer resistance (R_{et}).[32] The R_{et} value of the bare BDD was ca. 650 Ω. After MWCNT growth on BDD electrode, the semicircle domain (corresponding to R_{et}) was dramatically decreased to ca. 40 Ω (almost a straight line). It can be explained that the BDD/MWCNT electrode has very low R_{et} at the interface between electrode surface and electrolyte showing excellent electrocatalytic activity.

To calculate the effective surface area of the modified electrodes using the Randles-Sevcik equation, CVs were measured in a 3 M KCl solution containing 10 mM $K_3Fe(CN)_6^{3-/4-}$ at various scan rates. The peak currents (I_p) showed a linear relation with the square root of the scan rate ($v^{1/2}$) for both electrodes, as shown in Fig.7(c). This means that the reaction on each electrode is almost reversible and mainly diffusion-controlled with respect to the mass-transfer phenomenon in the double-layer region of the electrode. The Randles slopes of the bare BDD and BDD/MWCNT electrodes were 0.00115 (R = 0.99892) and 0.00168 (R = 0.99885), respectively. From these results, the effective surface area (A) of the BDD/MWCNT electrode was calculated as ca. 0.007158 cm^2, which is approximately 1.46 times larger than that of the bare BDD electrode because of the 3D-network porous structure of MWCNTs.

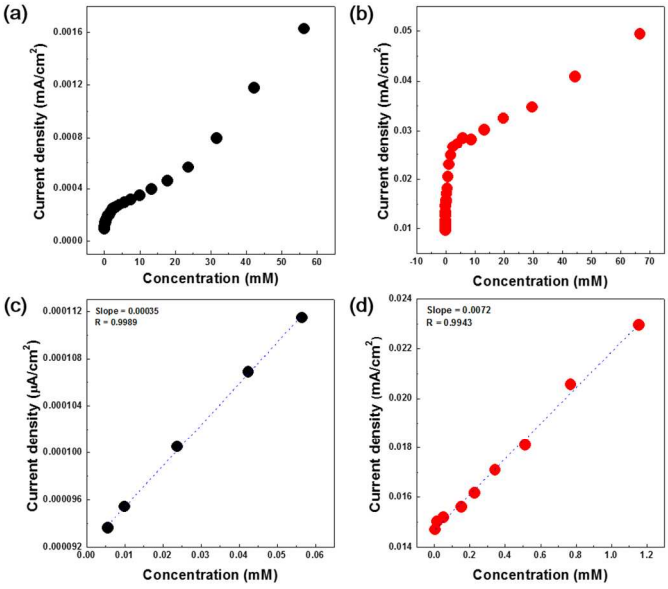

Figure 8. Full-range calibration curves of (a) the bare BDD electrode and (b) the BDD/MWCNT electrode for the glucose concentrations. Linear-range of the each electrodes; (c) the bare BDD electrode and (d) the BDD/MWCNT electrode.

Figure 8(a) and (b) show calibrated current versus glucose concentration curves for the bare BDD and BDD/MWCNT electrodes, along with the full-range data. For the bare BDD electrode (Fig.9(c)), the sensitivity was 0.35 μA/mM·cm^2 (R = 0.9989) with a linear range of 0.00565–0.0565 mM. The BDD/MWCNT electrode had a sensitivity of 7.2 μA/mM·cm^2 (R =

0.9943) in the linear range of 0.00565–1.1567 mM, as shown in Fig.9(d).

The reproducibility of the as-developed BDD/MWCNT electrode was measured at five different glucose concentrations as shown in Table 1. The relative standard deviation (R.S.D.) according to each concentration was below 4 % indicating the good reproducibility.

Table 2 shows the electrochemical biosensing performances for the amperometric glucose detection based on the BDD electrode modified with various nanoaterials.[33-36] Comparing the results, as-developed BDD/MWCNT electrode exhibits higher sensitivity with wider linear range and low detection limit than other modified electrodes. The combination of the MWCNTs having the large effective surface area and high electron transfer efficiency and the BDD having the low capacitive current and large potential window provided enhanced sensitivity over a wide linear range.

Table 1. R.S.D. values of the BDD/MWCNT electrode at each glucose concentration

Concentration [mM]	Current density [mA/cm^2]				R.S.D. [%]
	Sensor #1	Sensor #2	Sensor #3	Average	
1.1567	0.02295	0.02274	0.02363	0.02311	2.01
0.5141	0.01809	0.01775	0.01749	0.01777	1.69
0.22853	0.01617	0.0167	0.01744	0.01677	3.80
0.05079	0.01519	0.01441	0.01558	0.01506	3.96
0.00565	0.01469	0.01444	0.01395	0.01436	2.62

Table 2. Comparing results of amperometric glucose detection according to the modified materials on the BDD thin film

Electrode	Linear ranges [mM]	Detection Limit [μM]	Sensitivity	R	Ref.
BDD/GO_x	0.00565 – 0.0565	0.424	0.35 [μA mM^{-1}cm^{-2}]	0.9989	This work
BDD/PANI[a]/GO_x	0.347 – 13.33	68.5	1.39 [μA mM^{-1}]	0.9975	33
BDD/Pt-NPs[b]/GO_x	0.177 – 8.9	77.3	3.21 [μA mM^{-1}cm^{-2}]	0.9916	34
BDD/PANI/ Pt-NPs/GO_x	0.00594 – 0.514	0.102	5.54 [μA mM^{-1}]	0.9947	33
BDDP[c]/CoPc[d]/GO_x	0.2 – 1	-	3.9 [μA mM^{-1}]	-	35
BDD/X-APTES[e]-GO_x/Nafion	0.035 – 8	30	-	0.9983	36
BDD/ MWCNT/GO_x	0.00565 – 1.1567	0.0696	7.2 [μA mM^{-1} cm^{-2}]	0.9943	This work

a. Polyaniline
b. Platinum-nanoparticles
c. Screen printed boron-doped diamond powder
d. Cobalt phthalocyanine
e. 3-Aminopropyltriethoxysilane

Recently, non-invasive measurement of the glucose in human body using biofluids (i.e. saliva, tears, and sweat) has much attention for the indirect diagnosis of diabetes.[37] These sources include the glucose of which the concentration is lower than that of blood (micro molar range) and correlates with glucose concentration in blood. Although the linear range of the BDD/MWCNT electrode is not adequate for human body concentration (3–10 mM), it can be used for non-invasive measurement of the glucose concentration in saliva (~70 μM), tears (~200 μM), and sweat (~120 μM).[38] Consequently, the BDD/MWCNT electrode shows promise for biosensor application to detect the low concentration of biomolecules as well as non-invasive measurement of the glucose in living beings.

Conclusions

We demonstrated a method for site-selective and direct growth of MWCNTs on the BDD using electrostatically grafted SUS316L nanoparticles. MWCNTs were directly grown on the SUS316L nanoparticle as a catalyst-support. By using this method, the BDD/MWCNT electrode could be fabricated for electrochemical biosensor application. As-developed BDD/MWCNT electrode showed enhanced electrochemical performances and glucose sensing properties against the BDD electrode owing to their synergistic effect between the random networked MWCNTs and BDD.

Acknowledgements

This study was supported by the MSPI (The Ministry of Science, ICP and Future Planing), Korea, under the ICP R&D Infrastructure Support Program (NIPA-2014-I2218-13-1001) supervised by the NIPA (National IT Industry Promotion Agency); by grant No. RBD-0901-B0192-0 from the R&BD project of the Ministry of Knowledge Economy; by the Priority Research Centers Program (2009-0093823) through the National Research Foundation of Korea (NRF); by the Hi Seoul Science Fellowship from Seoul Scholarship Foundation; by the second stage of the Brain Korea 21 Project in 2012; and by the Korea University Grant.

Notes and references

[a] Dept. of Materials Science and Engineering, Korea University, Anam-Dong 5-1, Seoungbuk-gu, Seoul 136-713, Republic of Korea
[b] Dept. of Materials Science and Engineering, Yonsei University, 50, Yonsei-ro, Seodaemun-gu, Seoul 120-749, Republic of Korea
[c] Dept. of Technology and Society, The State University of New York, 119 Songdo Moonhwa-ro, Yeonsu-gu, Incheon 406-840, Republic of Korea
[d] These authors are contributed equal to this work
[*] Corresponding author: Phone: +82-2-3290-3272, Fax: +82-2-928-3584, Email: dslim@korea.ac.kr

1 M. Terrones, *Annu. Rev. Mater. Res.*, 2003, **33**, 419.
2 S. Park, M. Vosguerichian and Z. Bao, *Nanoscale*, 2013, **5**, 1727.
3 J. Whang, Electroanalysis, 2005, **7**, 17.
4 S. Vito and M. G. Dirk, *Chem. Soc. Rev.*, 2008, **38**, 165.
5 Y. Yun, Z. Dong, V. Shanov, W. R. Heineman, H. B. Halsall, A. Bhattacharya, L. Conforti, R. K. Narayan, W. S. Ball and M. J. Schulz, *Nano Today*, 2007, **2**, 30.

6 K. Balasubramanian and M. Burghard, *Anal. Bioanal. Chem.*, 2006, **385**, 452.
7 W. Yang, O. Auciello, J. E. Butler, W. Cai, J. A. Carlistle, J. E. Gerbi, D. M. Gruen, T. Knickerbonker, T. L. Lasseter, J. N. Russell Jr., L. M. Smith and R. J. Hamers, *Nature Mat.*, 2002, **1**, 253.
8 Hartl, E. Schmich, J. A. Garrido, S. C. R. Hernando, S. Walter, P. Feulner, A. Kromka, D. Steinmuller and M. Stutzmann, *Nature Mat.*, 2004, **3**, 736.
9 Stavis, T. L. Clare, J. E. Butler, A. D. Radadia, R. Carr, H. Zeng, W. P. King, J. A. Carlisle, A. Aksimentiev, R. Bashir and R. J. Hamers, *Proc. Natl. Acad. Sci. U. S. A.*, 2011, **108**, 983.
10 L. Tang, C. Tsai, W. W. Gerberich, L. Kruckeberg and D. R. Kania, *Biomaterials*, 1995, **16**, 483.
11 P. Si, Y. Huang, T. Wang and J. Ma, *RSC Adv.*, 2013, **3**, 3487.
12 J. Wang, J. Xue, J. Wang, J. Ye, H. Cui, F. Sheu and Q. Zhang, *Adv. Funct. Mater.*, 2005, **15**, 639.
13 T. A. Ivandini, R. Sato, Y. Makide, A. Fujishima and Y. Einaga, *Diam. Relat. Mater.*, 2004, **13**, 2003.
14 S. Szunerits, C. Jama, Y. Coffinier, B. Marcus, D. Delabouglise and R. Boukherroub, *Electrochem. Commun.*, 2006, **8**, 1185.
15 I. Shpilevaya, W. Smirnov, S. Hirsz, N. Yang, C. E. Nebel and J. S. Foord, *RSC Adv.*, 2014, **4**, 531.
16 Varshney, A. V. Sumant, B. R. Weiner and G. Morell, *Diam. Relat. Mater.*, 2012, **30**, 42.
17 N. Tumilty, L. Kasharina, T. Prokhoda, B. Sinelnikov and R. B. Jackman, *Carbon*, 2010, **48**, 3027.
18 Varanasi, J. Petry, L. Brunke, B. T. Yang, W. Lanter, J. Burke, H. Wang, J. S. Bulmer, J. Scofield and P. N. Barnes, *Carbon*, 2010, **48**, 2442.
19 B. T. Quinton, P. N. Barnes, C. V. Varanasi, J. Burke, B. Tsao, K. J. Yost and S. M. Mukhopadhyay, *J. Nanomater.*, 2013, **2013**, 356259.
20 C. Herbert, S. Ruffinatto, D. Eon, M. Mermoux, E. Gheeraert, F. Omenes and P. Mailley, *Carbon*, 2011, **52**, 408.
21 C. Stavis, T. L. Clare, J. E. Butler, A. D. Radadia, R. Carr, H. Zeng, W. P. King, J. A. Carlisle, A. Aksimentiev, R. Bashir and R. J. Hamers, *Proc. Natl. Acad. Sci. U. S. A.*, 2011, **108**, 983.
22 L. Tang, C. Tsai, W. W. Gerberich, L. Kruckeberg and D. R. Kania, *Biomaterials*, 1995, **16**, 483.
23 J. Rubio-Retama, J. Hernando, B. Lopez-Ruiz, A. Hartl, D. Steinmuller, M. Stutzmann, E. Lopez-Cabarcos and J. A. Garrido, *Langmuir*, 2006, **22**, 5837.
24 A. Shenderova, D. Areshkin and D. W. Brenner, *Mol. Simul.*, 2003, **29**, 259.
25 Varshney, A. V. Sumant, B. R. Weiner and G. Morell, *Diam. Relat. Mater.*, 2012, **30**, 42.
26 S. J. Sque, R. Jones, S. Oberg and P. R. Briddon, *Phys. Rev. B*, 2007, **75**, 115329.
27 N. Tumilty, L. Kasharina, T. Prokhoda, B. Sinelnikov and R. B. Jackman, *Carbon*, 2010, **48**, 3027.
28 S. Lee, J. Kim, M. Jeong, M. Song and D. Lim, *Nanotechnology*, 2010, **21**, 505302.
29 V. R. Sarath Babu, M. A. Kumar, N. G. Karanth and M. S. Thakur, *Biosens. Bioelectron.*, 2004, **19**, 1337.
30 X. H. Nguyen, Y. B. Lee, C. H. Lee and D. Lim, *Carbon*, 2010, **48**, 2910.
31 B. C. Liu, S. C. Lyu, T. J. Lee, S. K. Choi , S. J. Eum, C. W. Yang, C. Y. Park and C. J. Lee, *Chem. Phys. Lett.*, 2003, **373**, 475.
32 S. Upadhyay, G. R. Rao, M. K. Sharma, B. K. Bhattacharya, V. K. Rao and R. Vijayaraghavan, *Biosens. Bioelectron.*, 2009, **25**, 832.
33 M. J. Song, J. H. Kim, S. K. Lee, J. H. Lee, D. S. Lim, S. W. Hwang and D. Whang, *Microchim. Acta*, 2010, **171**, 249.
34 M. J. Song, J. H. Kim, S. K. Lee and D. S. Lim, *Anal. Sci.*, 2011, **27**, 985.
35 T. Kondo, M. Horitani, H. Sakamoto, I. Shitanda, Y. Hoshi, M. Itagaki and M. Yuasa, *Chem. Lett.*, 2013, **42**, 352.
36 Y. -F. Bai, T. -B. Xu, J. H. T. Luong and H. -F. Cui, *Anal. Chem.*, 2014, **86**, 4910.
37 Y. Kostov, X. Ge, G. Rao and L. Tolosa, *Meas. Sci. Technol.*, 2014, **25**, 015701.
38 J. C. Claussen, A. Kumar, D. B. Jaroch, M. H. Khawaja, A. B. Hibbard, D. M. Porterfield and T. S. Fisher, *Adv. Func. Mater.*, 2012, **22**, 3399.

Table of contents

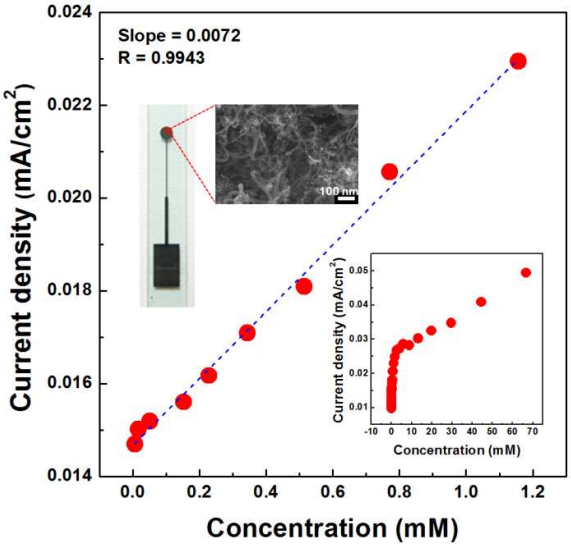

Selective growth of the MWCNTs on boron-doped diamond electrode was introduced and its electrochemical properties and glucose biosensing performances were reported.